How Aging Shapes Neural Representations of Space: fMRI Evidence for Broader Direction Tuning Functions in Older Adults

Christoph Koch (koch@mpib-berlin.mpg.de)[1], Shu-Chen Li[2] (Shu-Chen.Li@tu-dresden.de), Thad Polk[3] (tpolk@umich.edu) & Nicolas W. Schuck[1,4] (schuck@mpib-berlin.mpg.de)

[1]Max Planck Research Group NeuroCode, Max Planck Institute for Human Development, Lentzeallee 94, Berlin 14169, Germany
[2]Faculty of Psychology, TU Dresden, Zellescher Weg 17, Dresden 01069, Germany
[3]Department of Psychology, University of Michigan, 500 S State St, Ann Arbor, MI 48109, USA
[4]Max Planck UCL Centre for Computational Psychiatry and Ageing Research, Berlin, 14195 Berlin, Germany

Abstract

Human aging is characterized by losses in spatial cognition as well as reductions in distinctiveness of category-specific fMRI activation patterns. One mechanism linking theses two phenomena could be that broader neural tuning functions lead to more signal confusions when tuning-based representations of walking direction are read out. To test this idea, we developed a novel method that allowed us to investigate changes in fMRI-measured pattern similarity while participants navigated in different directions in a virtual spatial navigation task. We expected that adjacent directions are represented more similarly within direction sensitive brain areas, reflecting a tuning-function-like signal. Importantly, heightened similarity might lead downstream areas to become more likely to confuse neighboring directions. We therefore analyzed predictions of a decoder trained on these representations, asking (1) whether decoder confusions between two directions increased proportionally to their angular similarity, (2) and how this differs between age groups. Evidence for tuning-function-like signals was found in the retrosplenial complex and primary visual cortex. Significant age differences in tuning width, however, were only found in the primary visual cortex. Our findings introduce a novel approach to measure tuning specificity using fMRI and suggest broader visual direction tuning in older adults might underlie age-related spatial navigation impairments.

Keywords: fMRI; spatial navigation; MVPA; aging; neural dedifferentiation

Introduction

Many investigations in research on human aging have supported two major conclusions: Age-related memory impairment in humans is particularly pronounced in the domain of spatial navigation (Moffat, 2009) and accompanied by a loss of specificity in neural activation patterns, known as neural dedifferentiation (Li, Lindenberger, & Sikström, 2001). The later finding has often been likened to broadening of tuning curves of neural populations that have been observed in aged Rhesus monkeys, for instance in the visual domain (Leventhal, Wang, Pu, Zhou, & Ma, 2003). Neuronal tuning functions have been found in sensory, motor and spatial navigation-related areas, and universally are defined over a continuous variable that reflects the neural population's receptive domain, such as visual orientation. Age-related changes in tuning functions defined over continuous dimensions, however, have not been investigated in humans so far and their role in age-related changes in spatial navigation remains unclear.

In this study, we investigated age-related changes in the neural encoding of angular walking direction, a continuous space that is neurally represented by a set of directionally-tuned signals (Taube, 2007). We analyzed data of a previous study using a spatial memory paradigm (Schuck, Doeller, Polk, Lindenberger, & Li, 2015) to test if directional fMRI signals of older adults show evidence for broader tuning functions. Specifically, we asked (1) whether similarity of patterns gradually declines with larger angular differences, as predicted by directional tuning functions and (2) whether older adults show a broadened specificity of directional representations as suggested by the electrophysiological literature. Importantly, we assessed tuning functions based on the probability of a decoder to confuse neighboring directions, thus directly characterizing the effect broader tuning might have on downstream areas which have to decode represented information.

Materials and Methods

Participants and Task Data from 44 male participants (24 younger, $\mu_{age} = 27.87, \sigma_{age} = 4.01$; 20 older, $\mu_{age} = 67, \sigma_{age} = 3.82$) were included in the analyses. During the task participants navigated a three dimensional desktop-based virtual environment (VE) in first person view. The VE displayed a grass plane surrounded by a circular, non-traversable stone wall, distal orientation cues projected at infinite distance, and a landmark inside the arena in the form of a traffic cone. All movements in the VE were controlled using an MR-compatible joystick and exhibited constant speed. The experiment involved two runs. In each run of the task, participants first completed a phase to learn the location of five everyday objects placed in the arena. Afterwards, participants performed 30 trials in which the objects had to be placed at their learned location. During both of these phases participants could freely move through the arena. The third phase of each run involved changes of the environment and was therefore not included in the analysis. Further details about the task

can be found in Schuck et al. (2015).

Image acquisition and preprocessing Functional imaging data was acquired using a T2*-weighted echo-planar imaging (EPI) pulse sequence (3x3x3mm voxels, TR = 2400 ms, TE = 30 ms). All imaging data was preprocessed and analyzed using SPM12. The pipeline for each participant included spatial realignment, slice timing correction, coregistration to the anatomical scan and segmentation of the structural scan.

The analysis was focused on a set of ROIs connected to directional signals including the retrosplenial complex (RSC), the subiculum, a joint hippocampus and entorhinal cortex ROI, and the thalamus. As each direction is associated with visual input from a continuous scene a primary visual cortex (V1) ROI was included to capture visual direction effects. A ROI of the primary motor cortex (M1) was used to capture potentially spurious, motion-related effects on decoding, and served as a baseline.

Walking direction dependent fMRI signals The location and azimuth of a participant were logged every 100ms. In addition to the recorded azimuth, the angle of the vector connecting consecutive locations of the participant could be used to derive walking direction. Discrepancies of $180(\pm 20^{\circ})$ signaled backwards walking and were excluded from the main directional analysis. We segmented the continuous navigation into separate periods (events) during which participants' walking direction stayed within one of six discrete 60° bins for longer than 1 second.

Classification of walking direction was cross-validated based on half runs, yielding a total of four folds (2 halves of each of the two runs). Prior to decoder training, direction events were modelled fold-wise in two first-level general linear models (GLM, see below). In total each GLM included 24 directional regressors (4 folds times 6 direction bins), 6 motion regressors extracted during spatial realignment, and 2 run-specific mean signal level regressors.

Reduction of noise autocorrelation effects One main challenge for analyzing similarities of direction-related signals pertains to temporal autocorrelations. In particular, because neighboring walking directions are likely to appear close to each other in time, temporal autocorrelation of noise could account for similar neural patterns of similar walking directions. To reduce such effects on signal similarity, we temporally separated adjacent events using a "buffering" method. This comprised the separation of odd and even events into two data sets which were analyzed separately. In consequence, the buffered classifiers were trained on consecutive events which (1) were separated by at least 1 second (and often longer, $\mu = 10.83s$), and (2) mostly did not reflect neighboring directions. This dramatically reduced the similarity between neighboring directions that could be explained by temporally autocorrelated noise. Specifically, the autocorrelation between

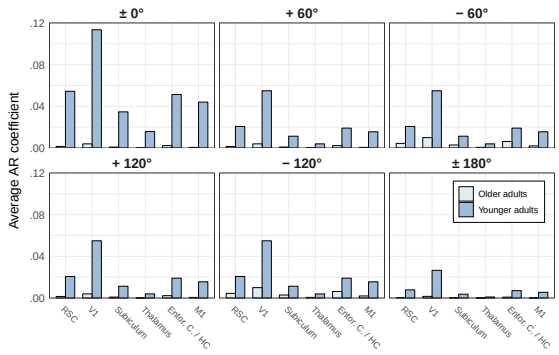

Figure 1: Average auto-correlation of signal for successive events after buffering. Specific for ROI and possible angular direction shifts between two successive events.

signals measured at consecutive TRs can be described by an 1-step *autoregressive model* in the form of

$$X_t = c + \varphi_1 X_{t-1} + \varepsilon_t. \quad (1)$$

, whereby φ_1, known as the AR(1) coefficient, expresses the relation between the signal at time t and the signal at X_{t-1}, and c and ε_t reflect constant and error terms, respectively. Based on Eqn. 1, the AR coefficient of the signal recorded p timesteps apart can be expressed as a exponential function of the AR(1) coefficient φ_1

$$\varphi_p = \varphi_1^p \quad (2)$$

Thus, because buffering increases the number of TRs separating two consecutive events, the autocorrelation between two events is reduced by an exponential factor of the additional TRs. To estimate this effect on the autocorrelation of the signal, we (a) estimated an AR(1) model on the intact data, (b) calculated the median number of TRs separating two consecutive events in the buffered GLM and (c) utilized Eqn. 2 to obtain the expected autocorrelation between two direction events. Average values of estimated autocorrelation for each possible direction change can be found in figure 1 and indicate negligible correlations mostly below .05.

Classification of walking direction A classifier (multi-class support vector machine, one-against-all, linear kernel) was trained on the directional beta maps of three folds and used to predict the direction associated with the beta maps in the hold-out fold. Classification accuracy was defined as the average number of correct predictions across all held out folds. Mean accuracy values across groups were statistically compared to M1 classification accuracy using a paired t-test (to ensure classification is above potentially spurious motion effects). Test statistics were adjusted for multiple comparisons using Bonferroni correction. ROIs in which classification accuracy exceeded the M1-baseline were entered into a comparison of three different but nested linear-mixed effects (LME)

models, all including a random effect of participant. Included fixed effects varied between the models: Model 1 included only a fixed effect of ROI, model 2 included fixed effects of ROI and age group, and Model 3 included an additional interaction between both. The three models were compared using an likelihood ratio test and followed up by post-hoc t-tests.

Tuning functions and neural broadening The classifier's confusion matrix (CM) reflects how often each category was decoded given a neural representation associated with each single category (e.g. how often did the classifier predict $120°$ although the participant walked into direction $60°$). By analyzing the CM, differences in representation similarity between two categories can be linked to their angular difference. In the case of a tuning function-based signal, the CM should be well approximated by a Gaussian bell curve that peaks at the target direction and decreases gradually with angular difference as the representations become less similar.

Within each buffer, each of the four cross-validation folds resulted in a curve describing the average proportion of classifier predictions for the correct (target) direction as well as each of the remaining off-target directions, i.e. $-120°$, $-60°$, $\pm 0°$, $+60°$, $+120°$, $\pm 180°$ relative to the target (all tuning functions were aligned by centering them to their respective true direction). Two models were fitted to the direction invariant CM of each participant. The first model captured the notion that of similarity gradually decreases with angular difference. This was approximated by a Gaussian curve given by

$$g(x) = \frac{1}{Z} e^{-\frac{1}{2}(\frac{x-c}{\sigma})^2}, \tag{3}$$

where x is a given direction, c is the center of the tuning function, $\frac{1}{\sigma}$ reflects the precision of the curve and $1/Z$ ensures normalization. Fixing c for each case to $\pm 0°$ allows to reinterpret x as simply reflecting the relative difference of the given direction from the center. In effect this model had only one free parameter, the precision.

We compared this model to a baseline model that assumed that all errors are evenly distributed. Values diverging from $\pm 0°$ were given by

$$u(x_{\neg 0°}) = \frac{100 - a}{5}, \tag{4}$$

which uniformly distributes the percentage remaining after subtraction of the value at the CMs center ($\pm 0°$), the free parameter a. Both models thus had only one free parameter were compared based on the sum of squared errors (SSE) between the model's prediction and the CM. Importantly, decoding values for the CM's center were excluded from the analysis. This step (a) renders the tuning function shape analysis independent from overall decoding accuracy and (b) avoids a bias towards the second model, since here the error would be zero by definition. To test if the CM is best described by a Gaussian model, participant-specific SSE values for both models were entered into a one-sided, paired t-test specific to each investigated ROI. Test statistics were adjusted for multiple comparisons using Bonferroni correction.

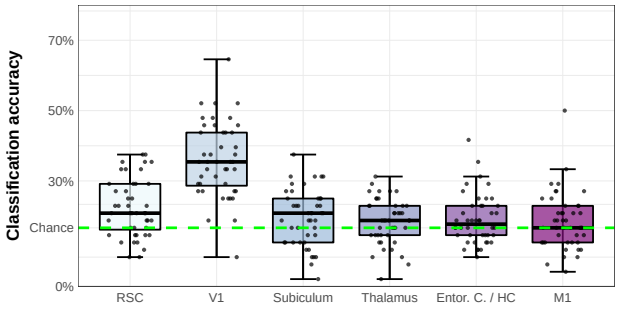

Figure 2: Classification accuracy averaged over both buffers. The dotted line indicates chance level classification accuracy of 16.6% resulting from six possible predictions, one for each direction.

Participant-specific measures for precision were extracted from the Gaussian model fitted to the CM. Prior to testing for higher precision in younger adults, distributions were tested for violating assumptions of normality due to smaller within group sample size. Tests for group comparisons were chosen accordingly. This analysis only considered ROIs showing evidence for both, classification accuracy above M1-baseline and tuning function-like signal.

Results

Classification accuracy of walking direction Classification accuracies for each ROI can be found in figure 2. The comparison to an M1-baseline showed significant decoding above M1 classification levels in the RSC- and V1 mask (all $p \leq .023$, Bonferroni corrected), but not in the thalamus or hippocampus masks ($p = .500$ and $ps \geq .232$, respectively). Model 1 showed that decoding tended to be bigger in younger adults (main effect of age group: $p < .001$). Model 2 indicated that decoding was generally higher in V1 than RSC (increased model fit when ROI was included: $p < .001$). The addition of an interaction term in Model 3 did not further improve model fit ($p = .072$), but a post-hoc t-tests revealed a significant difference between age groups only in V1 ($p < .001$, Bonferroni corrected), but not RSC ($p = .086$, Bonferroni corrected).

Shape of confusion matrix and tuning precision The classifiers predictions were captured in the CM. Model comparison based on SSE score across groups revealed that the Gaussian curve fitted the classifier's CM better than the opposing model in the RSC, V1, and the thalamus (all $p \leq .024$, Bonferroni corrected). As classification accuracy in the thalamus did not exceed an M1-baseline and might therefore be only due to spurious motion artifacts, Gaussian precision was investigated for age differences only in the RSC and V1. Assumption of normality was violated in younger adults in the V1 as indicated by a Kolmogorov-Smirnov test ($p < .001$).

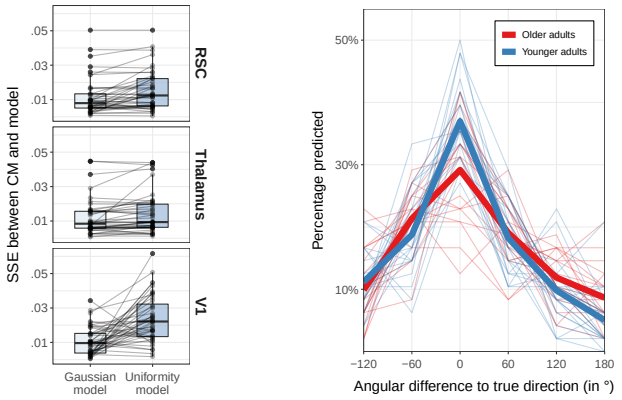

Figure 3: **Left:** Comparison of SSE values between both models arising from their fit to the individual CM in the RSC, Thalamus, and V1. **Right:** Average confusion matrix of younger and older adults in V1.

A Wilcoxon rank sum test indicated significantly higher precision in younger adults ($p = .042$, Bonferroni corrected). No evidence for non-normality or age-group differences in tuning width were found in the RSC. SSE comparison and averaged confusion matrices in V1 are shown in figure 3.

Discussion

In this study we used fMRI to investigate age-related changes in the specificity of neural direction-selective signals. More specifically, we asked if similarity of patterns gradually declines with larger angular differences, as predicted by directional tuning functions and whether older adults show broadened specificity of directional representations.

Our results revealed that directional information was decodable in the RSC and V1, in line with previous investigations (Shine, Valdés-Herrera, Hegarty, & Wolbers, 2016). Interestingly, age differences in decoding accuracy could only be found in V1. Going beyond mere accuracy, we introduced a novel method to characterize tuning function-like signals during decoder readout. This analysis demonstrated that, independent of overall classification accuracy, decoder confusions were approximated best by a Gaussian tuning function, indicating a gradual decline of pattern similarity in the RSC, thalamus, and V1, but not M1. Analyzing the width of the fMRI-level tuning function proxy given by the Gaussian model fitted to the CM indicated broadened specificity of directional representations in V1, where the Gaussian curve was significantly wider in older adults. In line with our predictions, this poses evidence for broader tuning functions in older adults as suggested by the neural broadening hypothesis.

To the best of our knowledge, this is the first study to investigate potential age-related changes in tuning functions defined over a continuous domain, rather than using discrete categories (Park et al., 2012). By applying the continuous variable of direction, the claims made by the neural broadening hypothesis concerning the change of tuning functions with age, which are only defined over continuous space, could be tested more specifically and are shown to converge with previous findings.

While it is likely that the measured signal in the RSC or thalamus contains directional information influenced by head direction cells (Shine et al., 2016), effects in the V1 are most likely based on visual inputs drawn from a continuous visual scene. Our results suggesting neural broadening in the early visual system converge with findings in single cell recordings demonstrating wider tuning functions in senescent monkeys confronted with a visual stimulus of various orientations (Leventhal et al., 2003). Given the sufficiently low-level of orientation signalling in the visual hierarchy it is possible that this process drives the present findings in V1 and suggests that the introduced method to investigate neural broadening might be sensitive to tuning curve related changes. Our results furthermore indicate that a classifier's CM can pose as a tuning function proxy measure of a continuous variable, providing a novel measure for neural specificity beyond classification accuracy. To see if the findings are specific to the investigated domains, the method should also be applied to other continuous variables, e.g. the perception of motion (Liang et al., 2010).

References

Leventhal, A. G., Wang, Y., Pu, M., Zhou, Y., & Ma, Y. (2003). GABA and its agonists improved visual cortical function in senescent monkeys. *Science (New York, N.Y.)*, *300*(5620), 812–5.

Li, S.-C., Lindenberger, U., & Sikström, S. (2001). Aging cognition: from neuromodulation to representation. *Trends in Cognitive Sciences*, *5*(11), 479–486.

Liang, Z., Yang, Y., Li, G., Zhang, J., Wang, Y., Zhou, Y., & Leventhal, A. G. (2010). Aging affects the direction selectivity of MT cells in rhesus monkeys. *Neurobiology of Aging*, *31*(5), 863–873.

Moffat, S. D. (2009). Aging and Spatial Navigation: What Do We Know and Where Do We Go? *Neuropsychology Review*, *19*(4), 478–489.

Park, J., Carp, J., Kennedy, K. M., Rodrigue, K. M., Bischof, G. N., Huang, C.-M., ... Park, D. C. (2012). Neural Broadening or Neural Attenuation? Investigating Age-Related Dedifferentiation in the Face Network in a Large Lifespan Sample. *Journal of Neuroscience*, *32*(6), 2154–2158.

Schuck, N. W., Doeller, C. F., Polk, T. A., Lindenberger, U., & Li, S. C. (2015). Human aging alters the neural computation and representation of space. *NeuroImage*, *117*, 141–150.

Shine, J. P., Valdés-Herrera, J. P., Hegarty, M., & Wolbers, T. (2016). The Human Retrosplenial Cortex and Thalamus Code Head Direction in a Global Reference Frame. *The Journal of Neuroscience*, *36*(24), 6371–6381.

Taube, J. S. (2007). The Head Direction Signal: Origins and Sensory-Motor Integration. *Annual Review of Neuroscience*, *30*(1), 181–207.